SCALING LAWS FOR RADIAL FOIL BEARINGS

by

SRIKANTH HONAVARA PRASAD

Presented to the Faculty of the Graduate School of

The University of Texas at Arlington in Partial Fulfillment

of the Requirements

for the Degree of

MASTER OF SCIENCE IN AEROSPACE ENGINEERING

THE UNIVERSITY OF TEXAS AT ARLINGTON

December 2014

Acknowledgements

I am deeply indebted to Dr. Daejong Kim for helping me overcome roadblocks throughout the course of my graduate studies. This work would not have seen fruition without his guidance, patience and unwavering support. I would also like to thank Dr. Atilla Dogan and Dr. Bo Wang for obliging to be a part of my thesis defense committee. I would also like to acknowledge the financial support provided by Dr. Daejong Kim and the Department of Mechanical and Aerospace Engineering, University of Texas at Arlington.

Special thanks are due to all the people that have enriched my life by showing me the power of rational thought. The debates and discussions with my friends, colleagues and family have helped me grow intellectually and emotionally.

Finally, I would like to thank my family for the endless love, emotional support and encouragement and for helping me navigate tough times with ease.

November 24, 2014

Abstract

SCALING LAW FOR RADIAL FOIL BEARINGS

Srikanth Honavara Prasad, M.S.

The University of Texas at Arlington, 2014

Supervising Professor: Daejong Kim

The effects of fluid pressurization, structural deformation of the compliant members and heat generation in foil bearings make the design and analysis of foil bearings very complicated. The complex fluid-structural-thermal interactions in foil bearings also make modeling efforts challenging because these phenomena are governed by highly non-linear partial differential equations. Consequently, comparison of various bearing designs require detailed calculation of the flow fields (velocities, pressures), bump deflections (structural compliance) and heat transfer phenomena (viscous dissipation in the fluid, frictional heating, temperature profile etc.,) resulting in extensive computational effort(time/hardware).

To obviate rigorous computations and aid in feasibility assessments of foil bearings of various sizes, NASA developed the “rule of thumb” design guidelines for estimation of journal bearing load capacity. The guidelines are based on extensive experimental data.

The goal of the current work is the development of scaling laws for radial foil bearings to establish an analytical “rule of thumb” for bearing clearance and bump stiffness. The use of scale invariant Reynolds equation and experimentally observed NASA “rule of thumb” yield scale factors which can be deduced from first principles. Power-law relationships between: a. Bearing clearance and bearing radius, and b. bump

stiffness and bearing radius, are obtained. The clearance and bump stiffness values obtained from scaling laws are used as inputs for Orbit simulation to study various cases.

As the clearance of the bearing reaches the dimensions of the material surface roughness, asperity contact breaks the fluid film which results in wear. Similarly, as the rotor diameter increases (requiring larger bearing diameters), the load capacity of the fluid film should increase to prevent dry rubbing. This imposes limits on the size of the rotor diameter and consequently bearing diameter. Therefore, this thesis aims to provide the upper and lower bounds for the developed scale laws in terms of the bearing diameter.

Table of Contents

List of Illustrations

List of Tables

Chapter 1

INTRODUCTION

A foil bearing is a device that supports rotating components in turbo-machinery systems through the action of fluid pressure generation between the rotating member and the bearing. The fluid pressurization could either be hydrostatic (using external pump) or hydrodynamic (self-acting). In hydrodynamic mode of operation, fluid pressurization occurs when there is asymmetrical relative motion between the rotor and the bearing top foil. Most commonly used fluid in foil bearings is air, though; any other process gas (e.g. helium, xenon) could be used depending on the application. In fact, these bearings could also be used in applications involving supercritical fluids (e.g. closed loop supercritical carbon dioxide S-CO2 Brayton Cycle). Therefore, the obvious benefits of gas foil bearings (GFB) include [1]:

Low weight: The absence of bulky oil systems reduces the payload in aerospace applications such as air cycle machines, bleed air turbo-compressors and turbo expanders.

High reliability: Hydrodynamic operation obviates potentially hazardous oil pressurization systems. Since fewer parts are required for operation, the maintenance and operating costs are reduced.

High temperature range: GFB systems can operate efficiently at very low temperatures and at very high temperatures. Conventional oil lubricated bearings do not offer such a broad temperature range of operation due to degradation of the oil at those temperatures.

High speed operation: GFB systems offer better efficiencies at higher operating speeds than conventional oil lubricated bearings.

In addition, due to tight tolerances in the design and assembly of foil bearings, the shaft assembly is restrained from excessive movement resulting in soft failures. However, the benefits of foil bearings can be fully exploited only when the bearing is able to demonstrate sufficient stability and competitive load capacity.

A typical foil bearing is shown in the Figure 1. A smooth foil constitutes the bearing surface (top foil) and that is supported by a corrugated sheet of metal foil (bump foil) which provides structural stiffness. The top foil and the bump foil retract under the action of hydrodynamic forces and form the compliant structure which is encased in a rigid stationary shell (bearing sleeve). In Figure 1 the gaps between the bump foil and the bearing sleeve and the bump foil and the top foil have been greatly exaggerated for clarity.

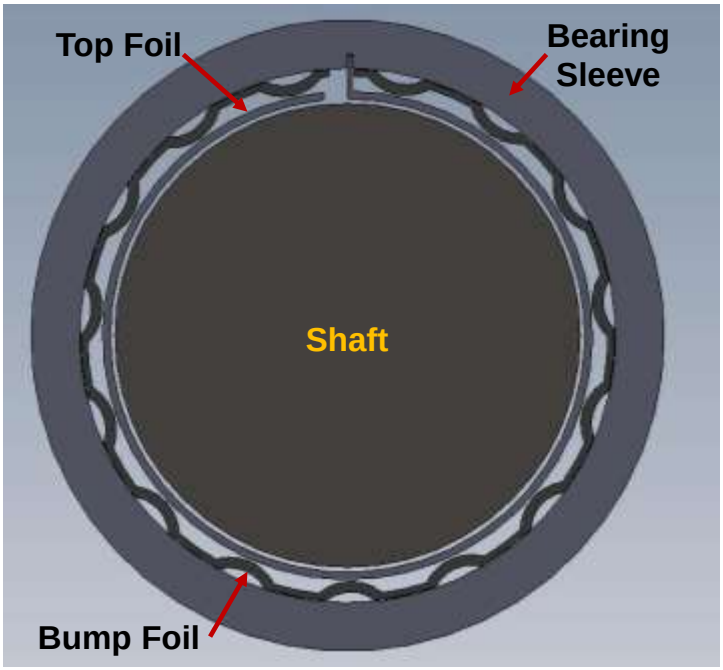

Figure 1 Typical foil bearing geometry for radial support (Journal Bearing)

The rotor is initially in weak contact with the bearing. As the rotor crosses a certain threshold speed (lift off speed), the fluid surrounding the rotor is drawn into the

convergent-divergent wedge between the rotor and the top foil resulting in formation of a fluid film. This fluid film physically separates the two entities and provides lubrication. The film occurs due to the effects of hydrodynamic forces (due to fluid viscosity and inertia associated with the total radial acceleration) which manifest as an asymmetrical pressure profile within the surrounding fluid. Thus, it is the asymmetrical pressure profile that supports the weight of the rotor [2]. The load that can be sustained by the fluid film without breaking is called the load capacity of the bearing. Since gases have low viscosity, the resulting pressure field tends to have lower load carrying capacity than oil-filled bearings.

Dry rubbing during start/stop operations of the rotor result in reliability issues for foil bearings. Therefore, surface coating with lubricant (Teflon-S, polyamide) is normally used to reduce friction during start/stop. Coulomb type damping exists between the top foil and bump foil and also between the bump foil and the bearing sleeve. The relative motions between the solid structures result in heat generation due to friction. Heat generation also occurs during high speed operation of the rotor through the mechanism of viscous dissipation in the fluid. Due to the low specific heat capacities of gases, parasitic heat generation within the bearing could result in localized thermal gradients compromising structural integrity [3]. Consequently, efficient cooling methods are required for thermal management, i.e., to prevent thermal runaway.

Therefore, the effects of fluid pressurization, structural deformation of the compliant members and heat generation in foil bearings make the design and analysis of foil bearing systems very complicated. The complex fluid-structural-thermal interactions in foil bearings make modeling efforts challenging because these phenomena are governed by highly non-linear partial differential equations. The hydrodynamic equation applicable to lubrication was first published by Osborne Reynolds in 1886 and is eponymously

called the Reynolds equation [4]. The Reynolds equation is obtained through simplifications of the Navier-Stokes momentum and continuity equations. The elastic deformations of the compliant structures are closely coupled to the stiffness and damping characteristics of the elastic members. The viscous heat generation and the temperature profile in the system are governed by the energy equation. These equations have to be simultaneously solved for specific geometries by using suitable initial and boundary conditions to analyze the performance of the bearing. The development of such models and their detailed numerical solutions require substantial effort and computational resources (time/hardware).

Consequently, comparison of various bearing designs require detailed calculation of the flow fields (velocities, pressures), bump deflections (structural compliance) and heat transfer phenomena (viscous dissipation in the fluid, frictional heating, temperature profile etc.,) which compound computational effort. To obviate rigorous computations and aid in feasibility assessments of foil bearings of various sizes, NASA developed the rule of thumb (ROT) design guidelines for estimation of journal bearing load capacity [5]. The guidelines are based on extensive experimental data and could be a useful starting point for developing other ROT's, i.e., for estimation of bearing clearance, stiffness and damping characteristics.

The scope of the current work is restricted to the development of scale laws for foil bearings using scale invariant Reynolds equation (non-dimensional) to establish a ROT for bearing clearance and bump stiffness. The non-dimensional Reynolds equation and the NASA ROT together yield scale factors which can be deduced from first principles. Power-law relationships between: a. Bearing clearance and bearing radius, b. bump stiffness and bearing radius, are obtained. The clearance and bump stiffness

values obtained from scaling laws are used as inputs for Orbit simulation to study various cases.

As the clearance of the bearing reaches the dimensions of the material surface roughness, asperity contact breaks the fluid film which results in wear. Similarly, as the rotor diameter increases (requiring larger bearing diameters), the load capacity of the fluid film should increase to prevent dry rubbing. This imposes limits on the size of the rotor diameter and consequently bearing diameter. Therefore, this thesis also aims to evaluate the upper and lower bounds for the developed scale laws in terms of the bearing diameter.

The organization of this thesis is based on the following outline. Literature review on air foil bearings is presented in Chapter 2. The literature review focuses on previous modeling efforts and describes the challenges in those efforts to demonstrate the need for simpler modeling guidelines. Chapter 3 discusses the theory of foil bearing as relevant to self-acting journal bearings. Chapter 4 introduces the scale law analysis which is followed by the methodology used in the current study to test the scale laws. Chapter 5 presents the results of the current study along with detailed discussion. Chapter 6 presents the conclusions of the study and explores the possibility of future work in this field.

Chapter 2

LITERATURE REVIEW ON FOIL BEARINGS

A number of researchers have developed analytical methods for the estimation of steady state load capacity in gas bearings [6-8]. Gross [9] indicates that exact solutions are available for certain types of self-acting gas bearings such as the plain wedge film, step-film and the taper-flat film. In those cases, the gradient of pressure normal to the flow direction is ignored due to infinite bearing assumption. Some authors have developed analytical solutions of finite bearings by invoking similar simplifying assumptions. In 1957, Ausman [6] developed a first order perturbation solution for the estimation of pressure, attitude angle and bearing stiffness by neglecting products of pressure variations and film-thickness variations. In 1961, he proposed an improved analytical solution [7] in which the product of pressure and film-thickness was treated as the dependent variable. The “Linearized PH” solution overcame certain deficiencies in his previous work but showed some discrepancy at high eccentricity ratios. In the same year, Gross and Zachmanoglou [8] developed perturbation solutions for large and small bearing numbers applied to journal and plane wedge films. They established limiting values of pressure and load for steady, self-acting, infinitely long bearings. In the method of perturbations, the existence of a solution for the dependent variable is assumed as a power series resulting in a series of linear equations. A reasonable approximation of the dependent variable can then be obtained by solving only the first few terms of the series. Many of the approximate solutions are based on linearization of differential equations to enable eigenvalue analysis [2].

With the advent of high speed digital computers, the use of numerical methods for solving the non-linear Reynolds equation applicable to the case of finite bearings gained impetus. Though the analytical solutions gave physical insight into the dominant

factors and general trends, numerical solutions offered much more accurate results. Raimondi [10] developed a series of numerical solutions for bearings of finite length based on the finite difference method (FDM). In the FDM, the governing equation is discretized and solved for a specified number of discrete points. A clear exposition of FDM in solving the lubrication problem along with several pertinent numerical procedures was provided by Michael [11]. Researchers elsewhere employed other numerical methods such as finite element method (FEM) or finite volume methods for obtaining solutions to the lubrication problem [12, 13].

In 1965, Cheng and Pan [14] used Galerkin's method to resolve the difficulty in handling the time dependent term for the stability analysis of self-acting, finite length journal bearing. The application of Galerkin's method allowed the reduction of the partial differential equation to a system of first order ordinary differential equations. The equilibrium solution was then obtained using Newton Raphson method. However, due to the limited terms employed in the Galerkin approximation, their results become erroneous in the high eccentricity ratio and low bearing number region.

In the same year, Castelli and Elrod [15] proposed a general bearing analysis method known as an "orbit method" in which the complete nonlinear equations were numerically integrated to obtain the shaft center orbits. In principle, this method has the effect of an "idealized experimental rig" or a "numerical rig" in which the fluid and motion equations are together marched in time. They employed finite difference discretization and Crank-Nicolson method for time integration. Due to the high computational costs involved, the Orbit method was only used to spot-check the stability threshold produced by a semi-numerical method, also developed by the same authors. The steady state results from the orbit method were compared with the positions and pressures obtained by Elrod and Burgdorfer [16] to remarkable agreement.

It is possible that the lack of sophisticated computers and the inability to perform quick calculations may have caused a general decline of research interest in the field of gas lubrication [17]. However, the interest in gas lubrication research was revived in the following decades due to the search for efficient slider bearing designs on computer peripheral devices [13] and through applications of foil bearings in Air Cycle Machines for aircraft pressurization and environment control [1]. In 1980, Adams [18] analyzed the response of a rotating flexible disk interacting with a read-write head. The coupled elasto-hydrodynamic (EHD) problem required simultaneous solutions of both the elasticity equations and the non-linear Reynolds equation at each iteration. However, they developed a method to eliminate the need for solving the Reynolds equation at each step and obtained significant savings in computational time.

Miller [19] notes that there are two distinct methods for the analysis of gas lubricated tribo-elements. The first method requires solutions of the equations of motion and the Reynolds equation at each time interval. This method is called the time-transient method and provides large amount of meaningful data. In the second method which is called the step jump approach, the gas film is assumed to exhibit linear response to successive, small step increases in the various degrees of freedom. Consequently, the Reynolds equation is solved only while generating the step response for each degree of freedom, while using analytic functions for the step response which yield closed form-solutions. This method eliminates lot of iterations and provides savings on computation time. In the step jump approach, the use of Laguerre polynomials for approximating the step response was one of the popular methods. However, they [19] determined that the use of Laguerre polynomials for approximating the step response may be inadmissible in some cases.

The earliest gas foil bearing designs were “tension dominated” tape-type bearings. Subsequently, all the foil bearings employed elastic foundations to support a compliant membrane (“bending dominated”) [20]. These bearings were tested for “proof of concept” turbo-compressors and turbo-generators [21]. Heshmat et al. [22] evaluated the performance of a gas foil bearing with spring supported compliant foil. They solved the Reynolds equations to determine the effects of various parameters on bearing behavior in both single and multi-pad configurations. Their work also discussed the desirable design features with regard to the bearing arc, selection of load angle, number of pads and degree of compliance.

Ku and Heshmat [23] presented a theoretical model of corrugated bump foil strip deformation considering the Coulomb damping between the bump foils and housing, the bump foils and the top foil, and also the local interactive forces between the bumps. They also investigated the effects of variable load distributions and the bump geometries on the stiffness of the bump foil strip and concluded that a high friction coefficient between top and bump foil results in increased coulomb damping and stiffness.

The same year, Peng and Carpino [24] calculated the stiffness and damping coefficients of an elastically supported foil bearing using a finite difference formulation. Their structural model used a thin and extendable material for the foil surface (negligible bending and inertia effects) .The Reynolds equation was solved using a modified forward iteration finite element method (developed by the same authors) to obtain steady state solutions. The authors noted that their prediction of the dynamic coefficients did not match the results from Heshmat [22]. The discrepancy was attributed to contrasting approaches used by the authors. Subsequently, Carpino [25] developed another finite element perturbation approach for an arbitrary bearing geometry with general fluid

properties and a complete structural model. Theoretical predictions of dynamic coefficients were presented for an air lubricated corrugated foil bearing.

Faria and San Andres [13] studied the high speed hydrodynamic gas bearing performance for plane and Rayleigh step slider bearings using both finite element and finite difference methods. They note that the flow equations for high bearing numbers become parabolic and conventional numerical methods produce oscillations in the solution. One way of tackling this difficulty is by employing control volume method with special schemes for the convective-diffusive flows. Alternately, efficient schemes could be developed within the finite element and finite difference methods to handle the numerical instability. Due to these difficulties, the authors studied upwind finite difference and finite element procedures and developed a novel finite element formulation based on the Galerkin weighted residual for convection-diffusion problems.

High speed rotor systems require adequate support stiffness and damping characteristics to achieve stable and low vibration operation. For compliant frictional dampers used in such systems, Salehi et al [26] developed a semi empirical model of the dynamic friction coefficient. The friction and damping characteristics were first obtained as a function of static load, frequency and amplitude of imposed vibration. Then, the frictional coefficients were derived empirically using two separate data evaluation techniques.

Pan and Kim [27] investigated the stability characteristics of a rigid rotor supported by a gas lubricated spiral-groove conical bearing. They used the method of infinitesimal narrow groove analysis (INGA) for the dynamic analysis of spiral groove bearing under steady load and generated stability threshold maps for axial, cylindrical and conical modes as functions of bearing numbers.

Song and Kim [28], designed, constructed and tested the hydrostatic air foil bearing (HAFB). Their experimental studies measured the load capacity, cooling capacity of hydrostatic operation and the drag torques during start/stops. They also developed an analytical model for top foil deflections using a 1-D analytical beam model and incorporated the effects of sagging under hybrid mode. The results were validated with experimental results in open literature. The top foil model was integrated with time-domain orbit simulations for parametric studies to predict imbalance response. Their study indicated that the bearing could suppress trans-critical vibrations but not the onset of hydrodynamic instability.

Further, Kim [29] conducted parametric studies on air foil bearings of two different configurations, i.e. circular and three-pad air foil bearings. The study indicated that the rotor-dynamic characteristics are much more sensitive to the overall bearing configuration than the stiffness and damping distribution in the elastic foundation.

It is very clear from the discussion that the modeling efforts of gas foil bearings are extremely difficult due to the highly non-linear nature of fluid-solid-thermal interactions. Consequently, some researchers have attempted to provide design guidelines that would obviate the need for detailed modeling and simulations. DellaCorte and Valco [5] related the load capacity of the bearing to the bearing size and operating speed from available data to obtain an empirical “Rule of Thumb”. This guideline allowed direct comparison of load capacities between various bearing designs without having to actually perform detailed simulations.

Chapter 3

FOIL BEARING THEORY

In Chapter 1, a brief introduction to foil bearings was presented. This chapter provides further insight into the theory of foil bearings using the example of a radial gas bearing. Figure 2 shows the cross section of a typical gas journal bearing under normal operating conditions. The shaded region represents the shaft of radius R and the outer circle represents the bearing which is separated by a thin fluid film of thickness h.

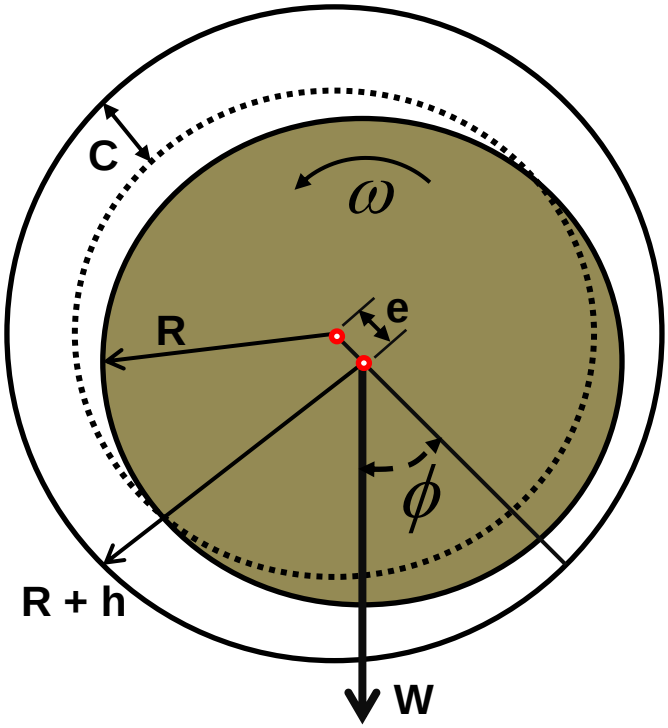

Figure 2 Schematic cross section of a typical journal bearing

In Figure 2, ω denotes the rotational speed in the direction of circumferential coordinate θ. The offset of the shaft center from the bearing center is denoted by the eccentricity e which is generally normalized by the clearance C and expressed as

"eccentricity ratio" $\in$. The bearing and the journal are fully concentric for $\in = 0$ and the rupture of film resulting in physical contact is described by $\in = 1$. The attitude angle ϕ is defined as the angle between the direction of bearing reaction force or applied load W and the eccentricity [2].

In Figure 2, the clearance between the shaft and the bearing has been greatly exaggerated. Though the clearance is a design feature, it is normally not observed in practice. Upon insertion of the shaft into the bearing, a weak contact (low contact pressure) is established between the foil assembly and the shaft. The dry friction experienced when the shaft is manually rotated, is the result of this weak contact which is often misinterpreted as a mechanical pre-load to the shaft. The existence of the weak contact can be traced to the unavoidable elastic spring back during cold forming and heat treatment despite the use of ideal tooling curvatures. However, if the bearing is subjected to a small hydrostatic force to gently push the loose foil assembly back to the bearing sleeve without causing deflection of the bumps, a finite bearing clearance is formed. This is the value of clearance used in numerical simulations.

The use of uniform clearance in bearing causes the rotor to become dynamically unstable at high rotation speeds. These instabilities result from large values of cross-coupled stiffness observed in lightly loaded gas bearings [30]. The instabilities are prominent in small diameter foil bearings and are amplified with the reduction in bearing size. The use of external loading to increase direct stiffness with respect to cross-coupled stiffness is not practical in very small rotating machines. Therefore, one of the methods employed in reducing the rotor instabilities is to design non-uniform bearing clearance. This is done by introducing multiple top and bottom foil structures or "multiple pads" within a single bearing sleeve shown in Figure 3.

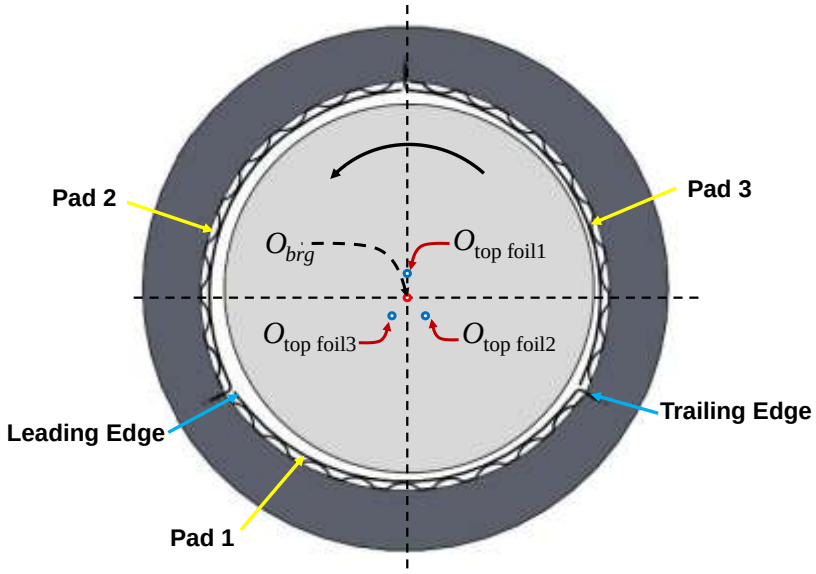

Figure 3 Three pad radial foil bearing

In Figure 3, a cross section of a multi-pad radial foil bearing consisting of 3 sets of top and bump foils within the sleeve is shown. The distance between the centers of the bearing O_{brg} and the top foils is called the hydrodynamic pre-load r_p which is associated with the hydrodynamic wedge effect described in Chapter 1. The amount of hydrodynamic preload is a design parameter based on the performance requirement of the bearing.

The determination of pressure profile is the most important step in bearing analysis. That is because the pressure profile reveals all other parameters of interest such as, the load capacity of the bearing, the forces and deflections in the elastic foundations, the friction forces, leakage etc. The governing equation for obtaining the pressures in gas foil bearing is the Reynolds equation for a compressible fluid. The equation is derived from simplifications of the Navier-Stokes equation substituted into the continuity equation. Therefore, a single partial differential equation with just two

dependent variables (pressure, channel height) represents all the three momentum equations and the continuity equation.

The following assumptions are common in the derivation of Reynolds equation [15] :

- Continuum flow of Newtonian fluid with constant viscosity
- Isothermal flow because of thin film and metallic boundaries
- Pressure variation across the film is not a dominant factor
- Viscous forces dominate over gravity and inertia

The non-dimensional compressible Reynolds equation in polar coordinates is written as [31]:

$$\frac{\partial}{\partial\theta}\left(PH^3\frac{\partial P}{\partial\theta}\right)+\frac{\partial}{\partial Z}\left(PH^3\frac{\partial P}{\partial Z}\right)=\Lambda\frac{\partial}{\partial\theta}(PH)+\sigma\frac{\partial}{\partial\tau}(PH) \tag{1}$$

Where,

$$\begin{aligned} P &= p/p_a & \theta &= x/R \\ Z &= z/R & H &= h/C \\ \tau &= \omega t \end{aligned} \tag{2}$$

Atmospheric pressure p_a, bearing radius R, clearance C and rotation speed ω are used in the non-dimensionalization of the governing equation. The non-dimensionalized Reynolds equation (1) reveals two important parameters, the bearing number Λ and the squeeze number σ which are defined as:

$$\Lambda=\frac{6\mu\omega}{p_a}\left(\frac{R}{C}\right)^2 \tag{3}$$

$$\sigma=\frac{12\mu\omega}{p_a}\left(\frac{R}{C}\right)^2=2\Lambda \tag{4}$$

The compressibility effects on bearing performance are captured by the bearing number (compressibility number) and the squeeze number. Bearing number relates the fluid compressibility and the sliding speed (describing the translational film characteristics) for hydrodynamic gas bearings. Similarly, the squeeze number describes the effect of squeeze film characteristics [9, 13, 32, 33]. Therefore, it has become customary to present the load capacities in terms of bearing number.

Once pressure is computed using equation(1), the load carrying capacities can be calculated:

$$F_X = -p_a R^2 \int_0^{2\pi} \int_0^{L/R} P(\theta, Z) \cos\theta \, d\theta \, dZ$$
$$F_Y = -p_a R^2 \int_0^{2\pi} \int_0^{L/R} P(\theta, Z) \sin\theta \, d\theta \, dZ \quad (5)$$

The film thickness observed during normal operation is the summation of the assembly clearance and the bump deflection $\delta(z,\theta)$:

$$h(z,\theta) = C(\theta) + e_x \cos\theta + e_y \sin\theta + \delta(z,\theta) \quad (6)$$

Equation (6) can be normalized using the nominal bearing clearance to yield:

$$H = 1 + \varepsilon_X \cos\theta + \varepsilon_X \sin\theta + S \quad (7)$$

Where, $\varepsilon = \frac{e}{C}$ and $S = \frac{\delta}{C}$ represent the eccentricity and normalized bump deflection respectively.

Chapter 4

SCALING LAWS AND METHODOLOGY

Development of Scaling Laws for Bearing Clearance

DellaCorte et al.[5] suggested from empirical observation of load capacities of various-sized foil bearings available to their research group that the load capacity of a bearing could be estimated based on the length L (in), diameter D (in) and shaft speed N (kilo-rpm) using the formula:

$$F = \alpha D^2 LN \tag{8}$$

Where, α is called the bearing capacity coefficient and it is a constant with the units $lbs \Big/ \left(in^3 \cdot krpm \right)$.

The load carrying capacity of a bearing in general case is given the integration of pressure over the bearing area:

$$F = \int P dA \tag{9}$$

This can be re-written in terms of pressure, bearing length and diameter as:

$$F = p_{avg} LD \tag{10}$$

We re-write the non-dimensional Reynolds equation using $P \dfrac{\partial P}{\partial Z} = \dfrac{1}{2} \dfrac{\partial P^2}{\partial Z}$ as:

$$\frac{\partial}{\partial \theta}\left(H^3 \frac{1}{2} \frac{\partial P^2}{\partial \theta} \right) + \frac{\partial}{\partial Z}\left(H^3 \frac{1}{2} \frac{\partial P^2}{\partial Z} \right) = \Lambda \left[\frac{\partial}{\partial \theta}\left(PH \right) + 2 \frac{\partial}{\partial \tau}\left(PH \right) \right] \tag{11}$$

Clearly, the LHS has pressure terms that are of order 2 and the RHS has pressure terms of order 1. Therefore, we can conclude:

$$P \propto \Lambda \tag{12}$$

It can also be concluded that integration of equation (11) over the domain of entire bearing would produce:

$$p_{avg} \propto \Lambda \tag{13}$$

Therefore, the average bearing pressure can be re-written in terms of bearing number(3):

$$p_{avg} \propto \Lambda = \left(\frac{6\mu\omega}{p_a}\right)\left(\frac{R}{C}\right)^2 \tag{14}$$

Equation (14) can be modified by expressing rotation speed in terms of rpm:

$$p_{avg} \propto \left(\frac{6\mu}{p_a}\frac{2\pi N}{60}\right)\left(\frac{R}{C}\right)^2 \propto N\left(\frac{\pi\mu}{5p_a}\right)\left(\frac{R}{C}\right)^2 \tag{15}$$

The result of (10) and (15) can be combined to express the load capacity as:

$$F = LDp_{avg} \quad \propto \quad N\left(\frac{\pi\mu}{5p_a}\right)\left(\frac{R}{C}\right)^2 \quad \propto \quad LD^2N\left(\frac{\pi\mu}{10p_a}\right)\left(\frac{R}{C^2}\right) \tag{16}$$

The term $\left(\frac{\pi\mu}{10p_a}\right)$ consists of constants and can be lumped under k_f which is the constant of proportionality. Therefore, the load capacity of the bearing can be expressed as:

$$F = k_f LD^2N\left(\frac{R}{C^2}\right) \tag{17}$$

For (17) to match the experimental scaling law suggested by DellaCorte et. al.[5] (8)

$$\alpha D^2LN = k_f LD^2N\left(\frac{R}{C^2}\right) \Rightarrow \alpha = k_f\left(\frac{R}{C^2}\right) \tag{18}$$

A very important conclusion can be drawn from equation(18). The ratio of the bearing radius to the square of the clearance is a constant value.

That is

$$\frac{R}{C^2} = \text{constant} \tag{19}$$

From (19) the estimation of clearance for different sized bearings using known values can be found:

$$\frac{R_1}{C_1^2} = \frac{R_2}{C_2^2} \qquad \Rightarrow \qquad C_2 = C_1\sqrt{\frac{R_2}{R_1}} \tag{20}$$

Development of Scaling Laws for Bump Stiffness

Bumps are modeled as a series of inertia-less linear springs;

$$f_b = k_b\delta + c_b\frac{d\delta}{dt} \tag{21}$$

In(21), the bump stiffness and equivalent bump viscous damping coefficient are k_b, c_b and the pressure force on the bump is given by $f_b = pA_0$. The effective area covered by the bump is $A_0 = 2\pi RL/N_{bump}$ where, N_{bump} represents the total number of bumps and L represents the length of the foil. If structural damping model is adopted for the foil structure, structural loss factor of bump η, bump stiffness k_b and the frequency of shaft motion ω_s yield the equivalent viscous damping coefficient:

$$c_b = \eta\frac{k_b}{\omega_s} \tag{22}$$

Equation (21) can be written in terms of pressure force on the bump and the structural loss factor as:

$$pA_0 = k_b\delta + \eta\frac{k_b}{\omega_s}\frac{d\delta}{dt} \tag{23}$$

Equation (23) can be written in normalized form as:

$$P = \frac{k_bCS}{p_aA_0} + \eta\frac{k_bC\omega}{p_aA_0\omega_s}\frac{dS}{d\tau} = \frac{k_bC}{p_aA_0}\left[S + \eta\frac{dS}{d\tau}\right] = K_b\left[S + \eta\frac{dS}{d\tau}\right] \tag{24}$$

Where, $P = \frac{p}{p_a}$, $S = \frac{\delta}{C}$, $t = \frac{\tau}{\omega}$ and $K_b = \frac{k_bC}{p_aA_0}$.

Consider equation(24), the steady state relation between non dimensional pressure and the scale invariant bump deflection becomes:

$$P = K_bS \tag{25}$$

The non-dimensional stiffness can be re-arranged as shown:

$$K_b = \frac{k_b C}{p_a A_0} = \frac{N_{bump}}{2\pi p_a}\left(\frac{C^2}{R}\right)\frac{k_b}{CL} = \frac{N_{bump}}{4\pi p_a}\left(\frac{C^2}{R}\right)\frac{k_b}{CR} \tag{26}$$

In equation(26), $L = D = 2R$ has been assumed. Using the result of(19), we can conclude that the right hand side of (26) is equal to product of constants (because $K_b = const$). Therefore:

$$\frac{k_b}{CR} = \text{constant} \tag{27}$$

Modification of (27) using the result of (19) yields:

$$\frac{k_b}{CR} = \text{constant} \quad \Rightarrow \frac{k_b}{CR}\left(\frac{C}{\sqrt{R}}\right) = \text{constant} \quad \Rightarrow \mathrm{k}_b \propto R^{1.5} \tag{28}$$

From (28) the estimation of bump stiffness using known values is very straight forward:

$$\frac{\mathrm{k}_{b,1}}{R_1^{1.5}} = \frac{\mathrm{k}_{b,2}}{R_2^{1.5}} \qquad \Rightarrow \qquad \mathrm{k}_{b,2} = \mathrm{k}_{b,1}\left(\frac{R_2}{R_1}\right)^{\frac{3}{2}} \tag{29}$$

The results from (20) and (29) are used for evaluating clearance and bump stiffness values for various bearing sizes based on a reference design. The values from scaling laws are used as input for Orbit simulation to find the zeroth order solution.

Chapter 5

RESULTS AND DISCUSSION

This chapter presents the details of reference design used for scaling laws. The results of Orbit simulations are also presented which include plots of stiffness, damping and eccentricity for various rotation speeds. Further, the pressure and film thickness profiles for highest rpm cases along with data on the maximum pressure and minimum film thickness for each test case is presented.

Reference Design

The turbo-machinery model used in the estimation of the total load on the bearing is shown in Figure 4. The model consists of compressor and turbine impellers (of equal mass), thrust runner, a hollow shaft and two sets of 3-pad radial foil bearings (preload 0.6 and offset ratio 0.5) that support the total load. The material of each component is assumed to be stainless steel of density 7850 kg/m^3.

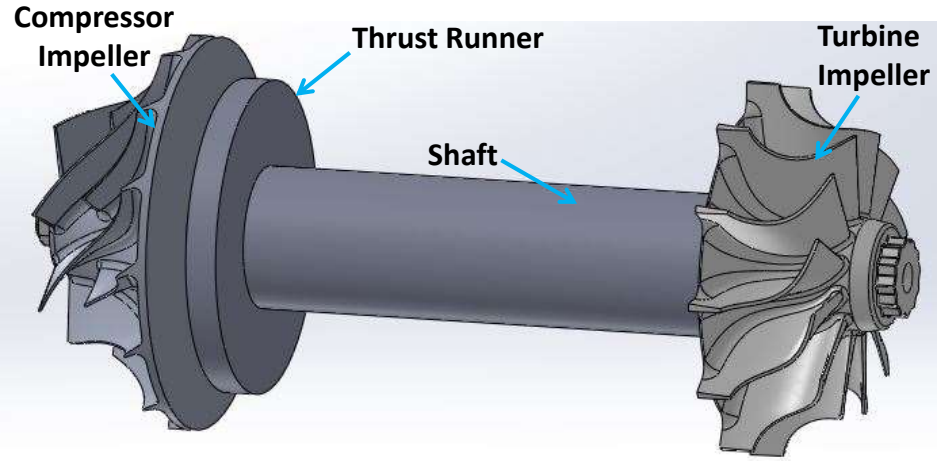

Figure 4 Turbo-machinery system considered for scaling

The reference model of turbo-machinery system was developed using commercial CAD software (SolidWorks) by adopting bearing OD 100 mm. All the remaining models were scaled up for higher bearing diameters and scaled down for lower

values of bearing diameter. A sectional view of the turbo-machinery system is shown in Figure 5 and the model of compressor impeller is shown in Figure 6.

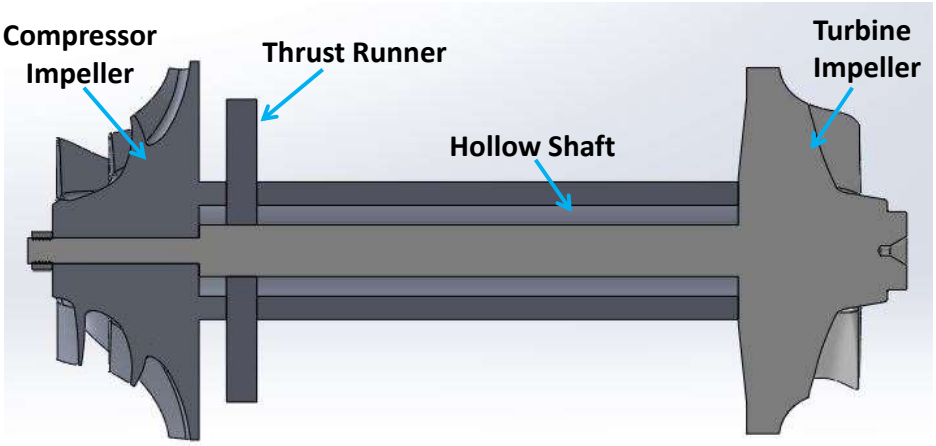

Figure 5 Sectional view of the turbo-machinery

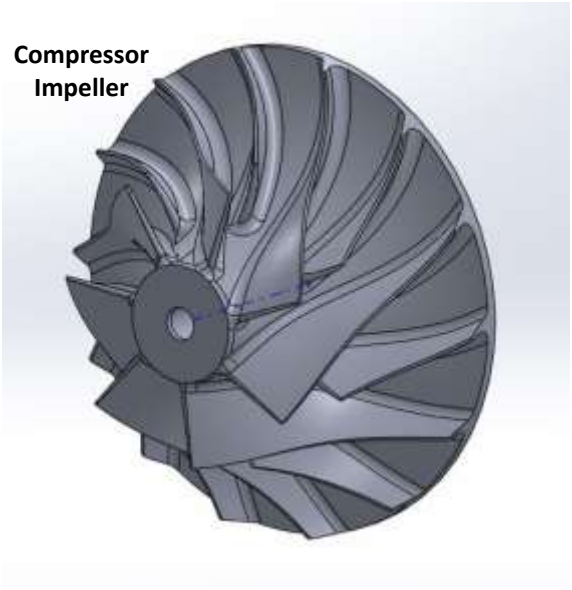

Figure 6 Compressor Impeller

The mass of the turbine impeller was chosen to be equal to the mass of the compressor impeller. The mass of turbine shaft was neglected in comparison to the total mass of rotor. The model of the turbine impeller and the turbine shaft is shown in Figure 7

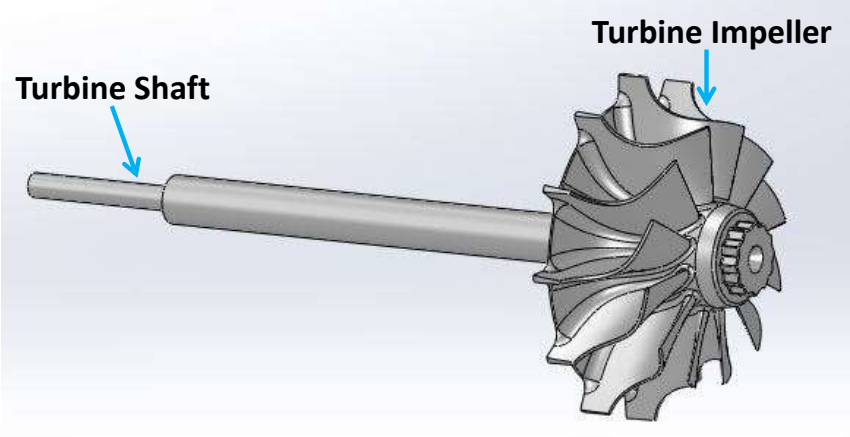

Figure 7 Turbine with turbine shaft

Based on available literature, the geometric relationships between component size and bearing size were assumed. Assuming bearing and the shaft OD to be D, the remaining geometric parameters were calculated based on the following assumptions:

- Bearing length is equal to the bearing OD
- Shaft inner diameter (ID) and the thrust runner ID = 0.66D
- Thrust runner OD = 2.2 D
- Thrust runner thickness/ thrust runner OD = 0.1
- Compressor impeller OD = 1.25 thrust runner OD

Therefore, for the case of Bearing OD = 100 mm (D), shaft OD = 100 mm (D), Bearing Length = 100 mm (D), shaft ID = 66mm (0.66 D), thrust runner ID = 66mm (0.66 D), thrust runner OD = 220mm (2.2 OD), thrust runner thickness = 22 mm, compressor impeller OD = 275 mm, Shaft length = 350 mm (3.5D). By suitable scaling of the solid

model, the dimensions of all components for various values of the diameters were obtained. The results are tabulated in Table 1.

Table 1 Dimensions of turbo-machinery components

Journal OD [mm]	Thrust Runner OD [mm]	Thrust Runner ID [mm]	Thrust Runner Thickness [mm]	Compressor Impeller OD [mm]	Shaft Length [mm]
20	44	13.2	4.4	55	70
50	110	33	11	137.5	175
75	165	49.5	16.5	206.25	262.5
100	220	66	22	275	350
150	330	99	33	412.5	525
200	440	132	44	550	700
250	550	165	55	687.5	875
300	660	198	66	825	1050

The mass of individual components and the total load (Table 2) was computed using the density information in the CAD software. The total load acting on both the bearings is due to the sum of thrust runner mass T_m, compressor and turbine impeller masses C_m and the shaft mass S_m. Therefore, the total load acting on each bearing M_{Brg} is half the sum of the total load acting on both the bearings.

$$M_{Brg} = \frac{2C_m + T_m + S_m}{2} \tag{30}$$

The unit pressure P_{unit} on bearing defined as the rotor weight per bearing over projected area (D^2) i.e., $P_{unit} = \frac{9.81 \cdot M_{Brg}}{101325 \cdot D^2}$ is also shown in Table 2.

Table 2 Mass estimation through scaling

Journal OD [mm]	Thrust Runner Mass [kg]	Compressor Impeller Mass [kg]	Shaft Mass [kg]	Total rotor mass [kg]	Rotor mass per bearing [kg]	Unit Pressure on bearing [bar]
20	0.05	0.13	0.1	0.41	0.205	0.050
50	0.75	2.01	1.52	6.29	3.145	0.122
75	2.52	6.78	5.14	21.22	10.61	0.183
100	5.97	16.06	12.18	50.27	25.135	0.243
150	20.16	54.21	41.1	169.68	84.84	0.365
200	47.79	128.5	97.43	402.22	201.11	0.487
250	93.34	250.98	190.3	785.6	392.8	0.608
300	161.3	433.69	328.84	1357.52	678.76	0.730

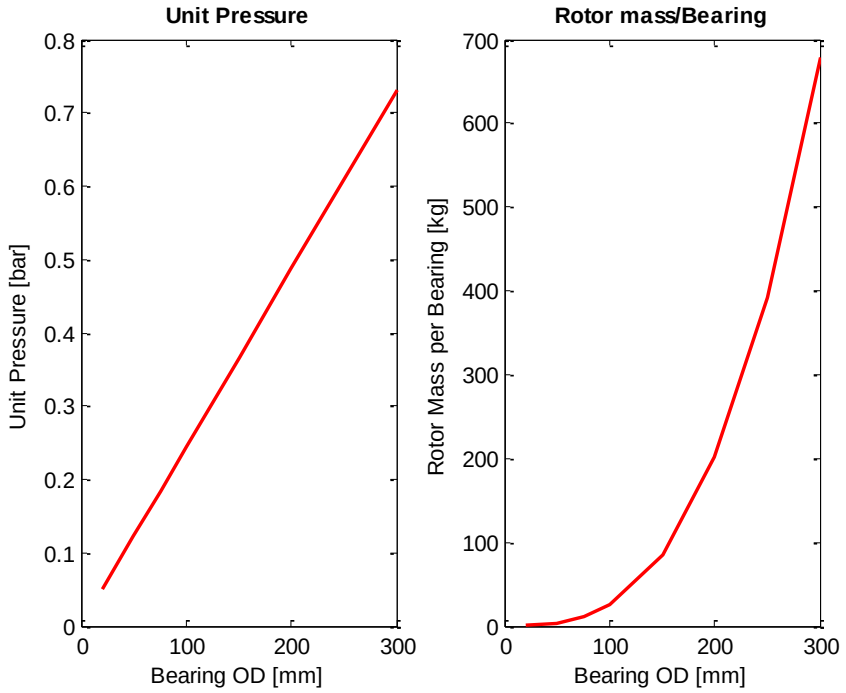

Figure 8 Unit pressure and Rotor mass per bearing versus bearing size

The unit pressure is a very important design criterion for bearings. From Figure 8, the unit pressure is a linear function of the bearing diameter. In contrast, the relationship between the rotor mass and bearing diameter is exponential.

Table 3 Clearance and Stiffness from the scaling laws

Journal OD [mm]	Clearance [μm]	Bump Stiffness [MN/m]
20	53.67	1.79
50	84.85	7.07
75	103.92	12.99
100	120.00	20.00
150	146.97	36.74
200	169.71	56.57
250	189.74	79.06
300	207.85	103.92

Table 4 Speed data for test cases

Journal OD [mm]	RPM_MIN					RPM_MAX
20	35000	63000	91000	119000	147000	175000
50	14000	25200	36400	47600	58800	70000
75	9333	16800	24267	31733	39200	46667
100	7000	12600	18200	23800	29400	35000
150	4667	8400	12133	15867	19600	23333
200	3500	6300	9100	11900	14700	17500
250	2800	5040	7280	9520	11760	14000
300	2333	4200	6067	7934	9800	11667

For the case of bearing OD=100 mm, the clearance was chosen to be 120 μm and the bump stiffness was assumed to be 20 MN/m. Similar values of clearance and bump stiffness can be found in literature for large bearing diameters. The values of clearance and bump stiffness for other bearing diameters shown in Table 3 were evaluated using the scaling laws developed in Chapter 5.

Assuming the DN number (product of diameter in mm and speed in RPM) = 3.5 million, the upper limits of the speed (RPM_MAX) were computed for the various cases of bearing diameters. The lower bound speeds (RPM_MIN) were assumed to be 5 times smaller than the respective upper limits. Therefore, the Orbit simulation was conducted 48 times for various bearing diameter and RPM values shown in Table 4. The simulations yielded values of stiffness, damping, eccentricity, pressures and film thickness for various bearing diameters.

Figure 9 and Figure 10 show the stiffness values plotted against speeds for various bearing diameters. It is clear from the plots that the values of direct stiffness k_{xx} increase considerably with increase in the size of bearing. A large bearing corresponds to a large (heavier) shaft. Therefore, higher k_{xx} is observed for large diameter bearings.

In small bearings Figure 9 (a. and b.), the relative contributions of all the stiffness components are of comparable magnitude. However, with increasing bearing size the k_{xx} value becomes much larger than the other stiffness counterparts. The slope of the direct stiffness k_{xx} continuously increases with increasing speeds for low bearing diameters (OD 20 mm). With increasing bearing diameter, the slope of the curve slowly begins to taper and at high bearing diameters (>OD 150 mm) the curve slopes downwards (Figure 10).

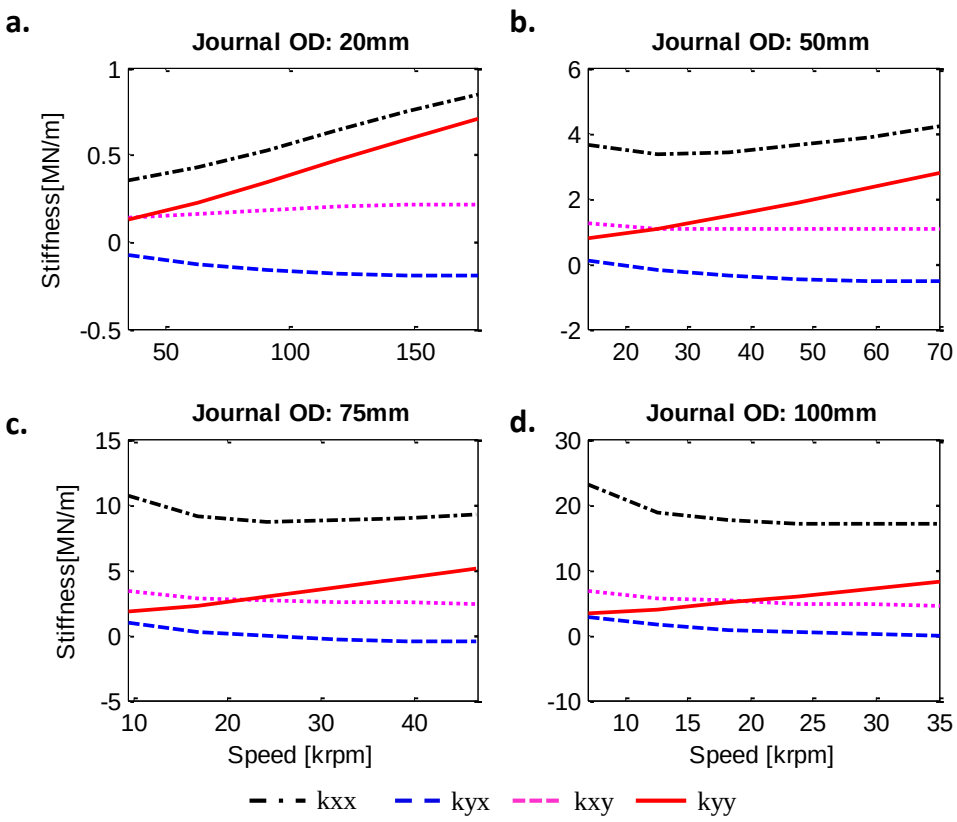

Figure 9 Stiffness versus Speed (Journal OD 20 mm – 100 mm)

This phenomenon is explained due to the effect of fluid pressurization and the relative contributions of the bearing stiffness for small and large bearings. The total stiffness of the bearing comes from the series stiffness effect of fluid film and the compliant structure. Consider the following cases using Table 6, Figure 13 and Figure 14 as reference:

Case 1: Speed is constant

The effect of increasing journal diameter keeping speed of rotation constant is that the maximum film pressure (P_max) increases and the minimum film thickness

(H_min) decreases. The displacement of journal also increases as indicated by higher eccentricity. This is easily attributable to the increase in mass of the journal.

Case 2: Diameter is constant

The effect of increasing journal rotation speed at a constant journal diameter is that the maximum film pressure decreases and the minimum film thickness increases. The displacement of the journal also decreases as indicated by decreased eccentricity. This result is attributed to increase in fluid being drawn into the wedge with increasing speed.

Case 3: Diameter and Speed are increasing

Finally, if the journal diameter and the speed are both increased from a reference value, competing effects between case 1 and case 2 decide the peak pressure, minimum film thickness and eccentricity values as shown in Table 5.

Table 5 Effects of journal diameter and speed

Journal OD [mm]	Speed [kRPM]	Eccentricity $\in$	P_max [bar]	H_min [μm]
Increase	Constant	Increase	Increase	Decrease
Constant	Increase	Decrease	Decrease	Increase
Increase	Increase	Compete	Compete	Compete

The total direct stiffness is the effect of the film pressure and the bump foil in series. The stiffness of the bump foil is almost constant and the stiffness is therefore dependent on the pressure. Clearly, for larger journal, the maximum pressure decreases with increasing speed (Table 6) which results in reduced stiffness. But it has to be noted that the absolute values of the direct stiffness for larger journal are still substantially larger than the smaller journal. It is only the trend that is shows decreasing stiffness values.

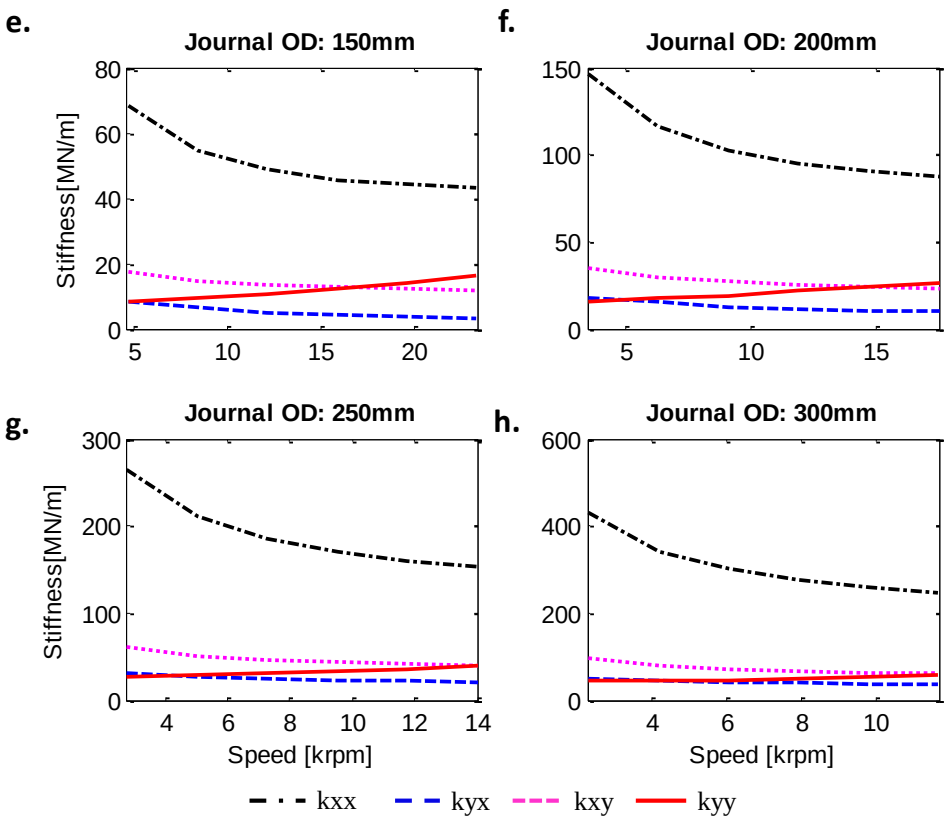

Figure 10 Stiffness versus Speed (Journal OD 150 mm – 300 mm)

The effects of increasing bearing size on direct stiffness k_{yy} and the cross coupled stiffness components k_{xy} and k_{yx} are less dramatic. However, it can be observed that their values continuously increase with increasing bearing size, as expected. The cross coupled components are of significance in foil bearings. This is because their presence and relative contributions to stiffness and damping determine the bearing instability. The cross coupling of two mutually perpendicular directions is explained for clarity.

Film pressurization is a reaction force mechanism to applied load on the fluid. However, since pressure is a scalar and does not have a preferred direction, the reaction

force on the rotor is directed such that there are force components in the radial and tangential directions.

When the rotor has finite mass, the pressure profile is such that any rotor displacement in horizontal direction produces a force in vertical direction or if there is a displacement in vertical direction, a force in horizontal direction is produced. This is the coupling of two mutually perpendicular directions and the presence of this coupling drives the rotor into orbit around the static equilibrium position.

But this orbit is limited by the clearance that exists between the rotor and the bearing. If the accelerations produced by the cross coupled force components become significantly large, the rotor might make physical contact with the bearing. Tilting pad bearings are known to mitigate these issues.

The cross coupled components of stiffness and damping can be positive or negative depending on the direction of reaction forces they produce relative to the direction of the coordinate axes.

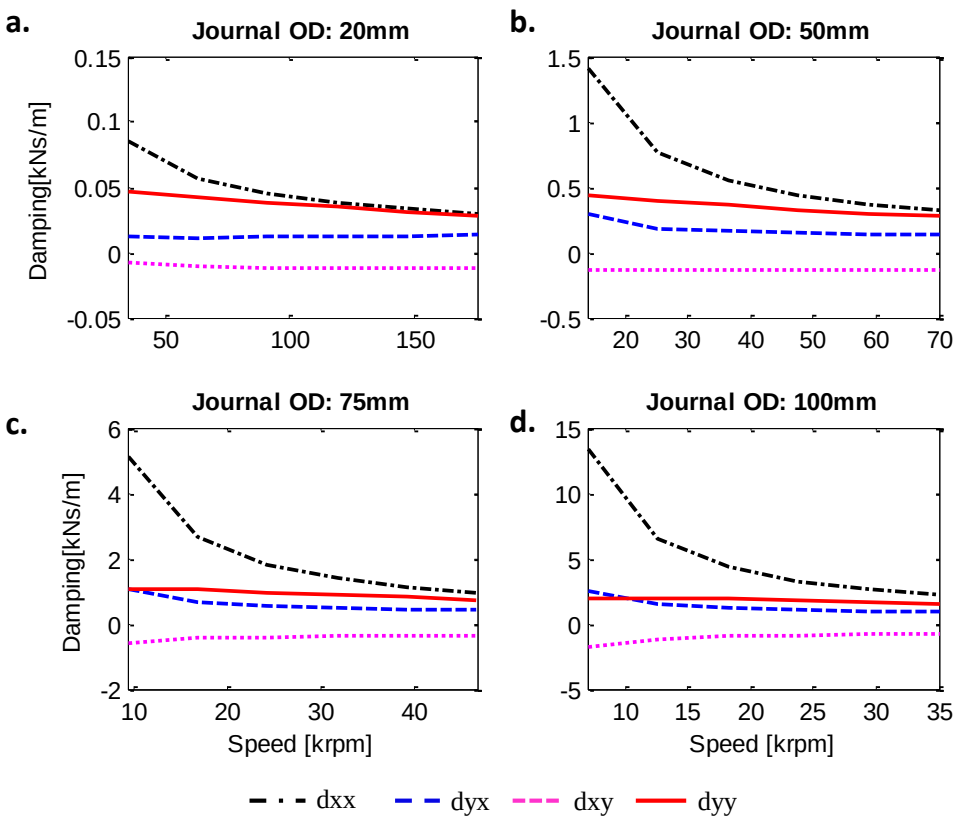

Figure 11 Damping versus Speed (Journal OD 20 mm – 100 mm)

The damping versus speed plots for various bearing sizes are shown in Figure 11 and Figure 12. Damping is the mechanism by which kinetic energy is dissipated. In dynamical systems such as foil bearings, damping occurs through various types of deformation, dissipation and chemical effects.

The trend observed for damping coefficient d_{xx} is similar to that of direct stiffness coefficient k_{xx}. Large values of d_{xx} are observed for low rotation speeds. However, as the rotation speeds increase, the direct damping coefficient shows a decreasing trend.

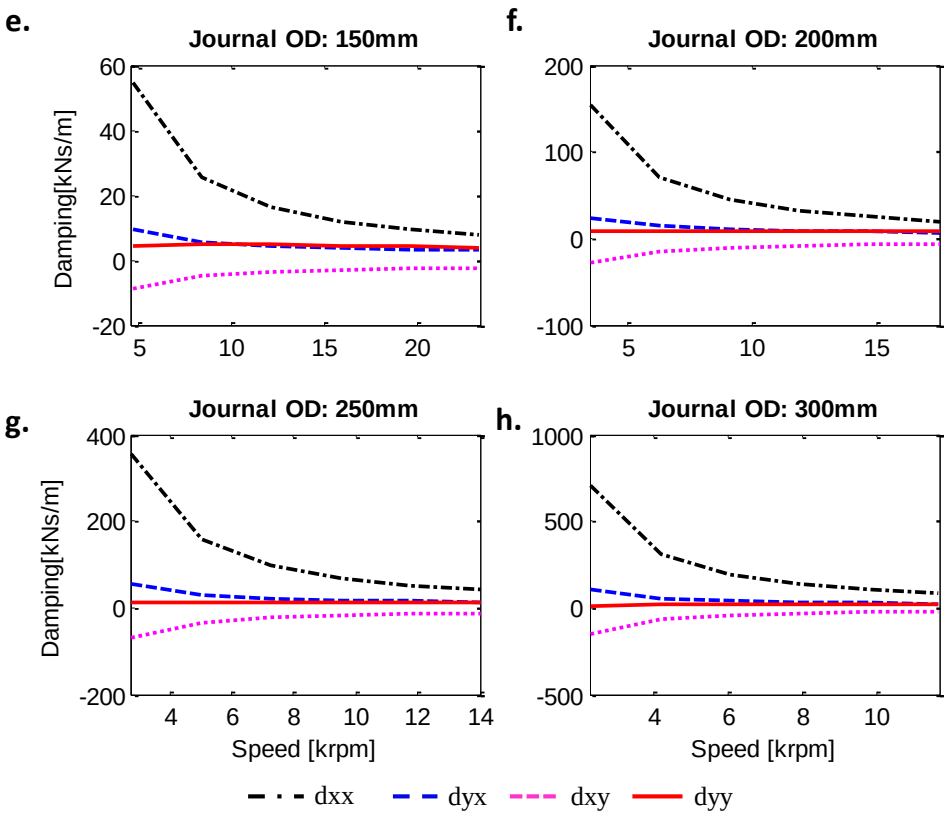

Figure 12 Damping versus Speed (Journal OD 150 mm – 300 mm)

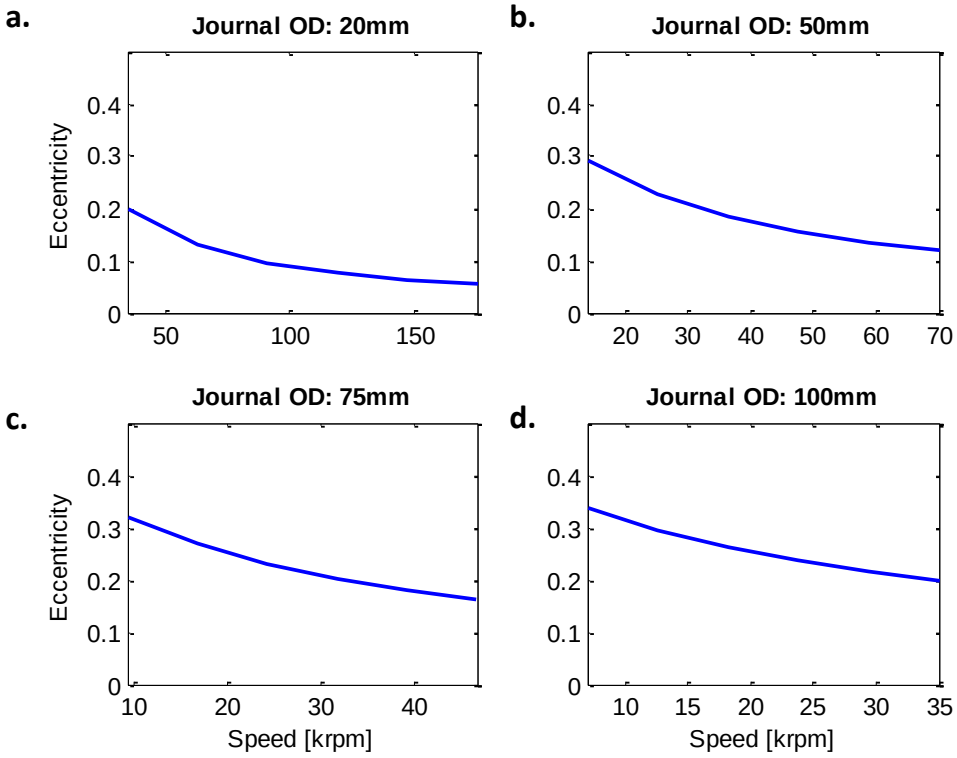

Figure 13 Eccentricity plot (Journal OD 20 mm – 100 mm)

The plots of eccentricity versus rotation speeds for various bearing sizes are shown in Figure 13 and Figure 14. It is observed that the eccentricity values are higher for larger diameter shafts. This is because the “squeeze effects” of large shafts strongly deform the film resulting in increased journal eccentricity. However, the eccentricity decreases with increasing rotation speed in each case. This is attributed to higher quantities of fluid being drawn into the wedge.

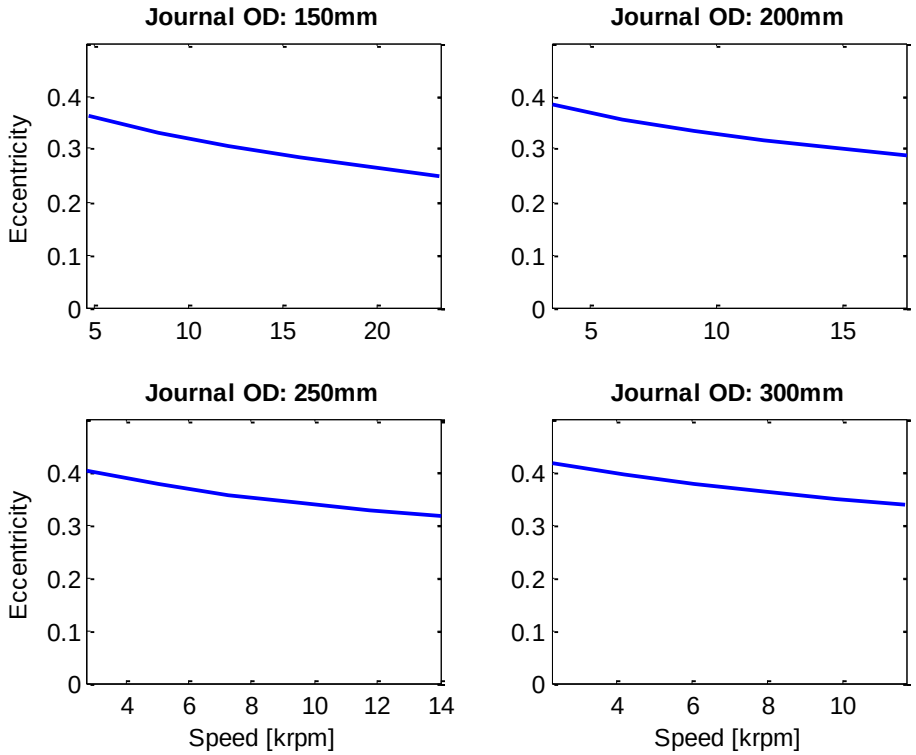

Figure 14 Eccentricity plot (Journal OD 150 mm – 300 mm)

The maximum pressure and minimum film thickness are plotted for highest rpm values for each bearing size (Figure 15 through Figure 30). The film pressures increase with increasing bearing size. Three distinct profiles are observed because of 3-pad configuration. As the bearing size increases, the asymmetry of loading results in dramatic pressure increase in the vertical direction. Therefore, the resulting profile is dominant in the center which corresponds to the bottom pad. The location of the minimum film thickness also corresponds to the bottom pad. Table 6 shows the values of minimum film thickness and maximum pressure for all the cases. The results are provided without any further comments.

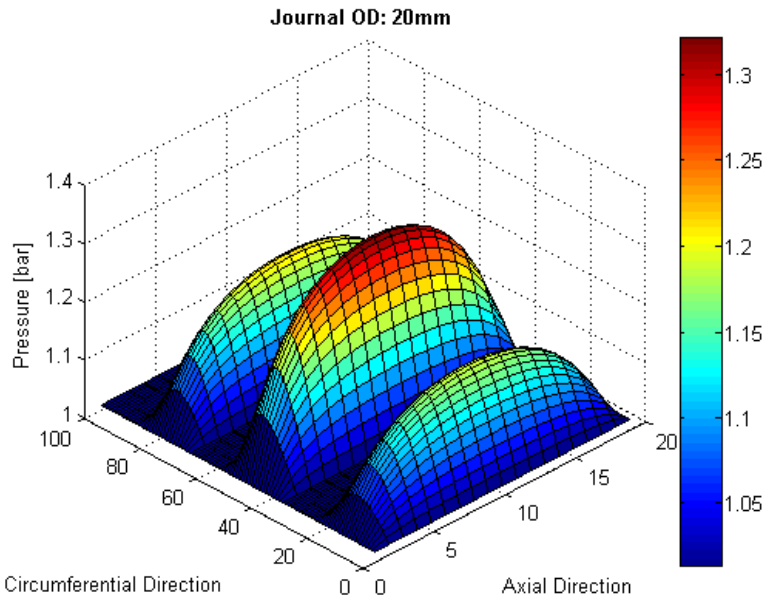

Figure 15 Pressure profile (Journal OD 20 mm and Speed 175 krpm)

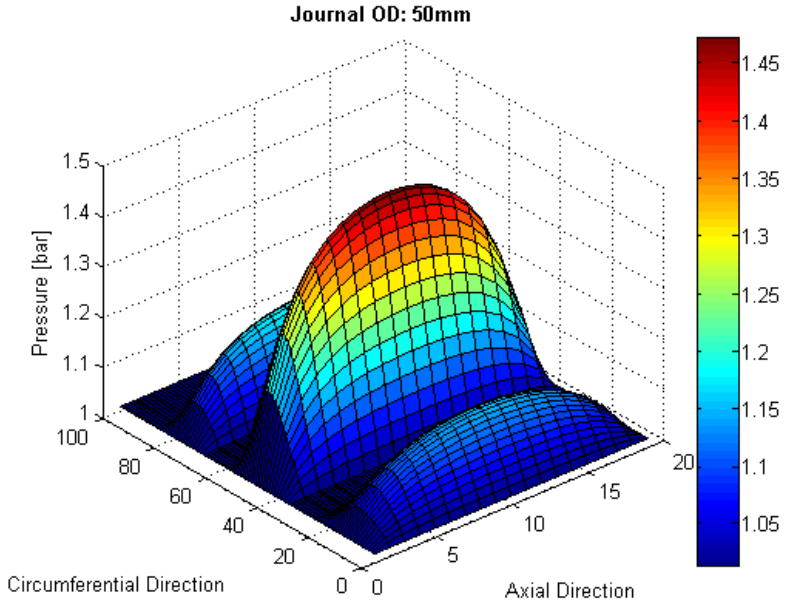

Figure 16 Pressure profile (Journal OD 50 mm and Speed 70 krpm)

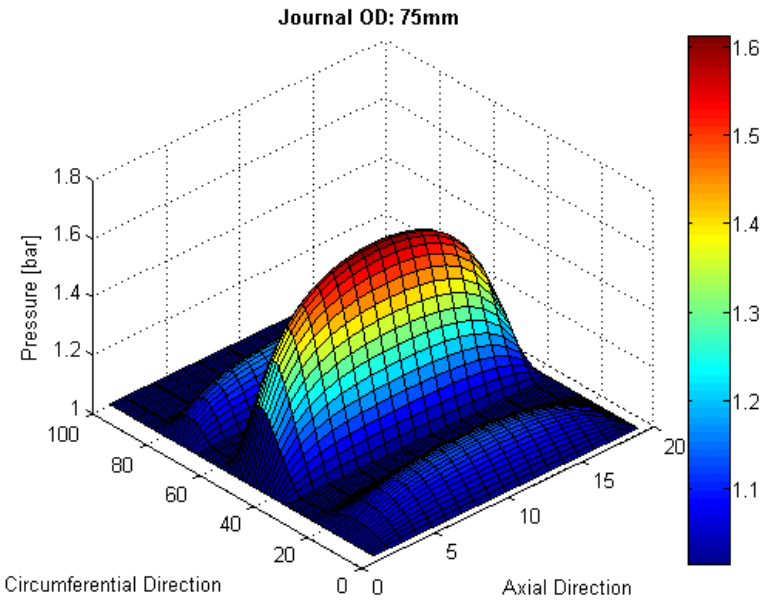

Figure 17 Pressure profile (Journal OD 75 mm and Speed 46.67 krpm)

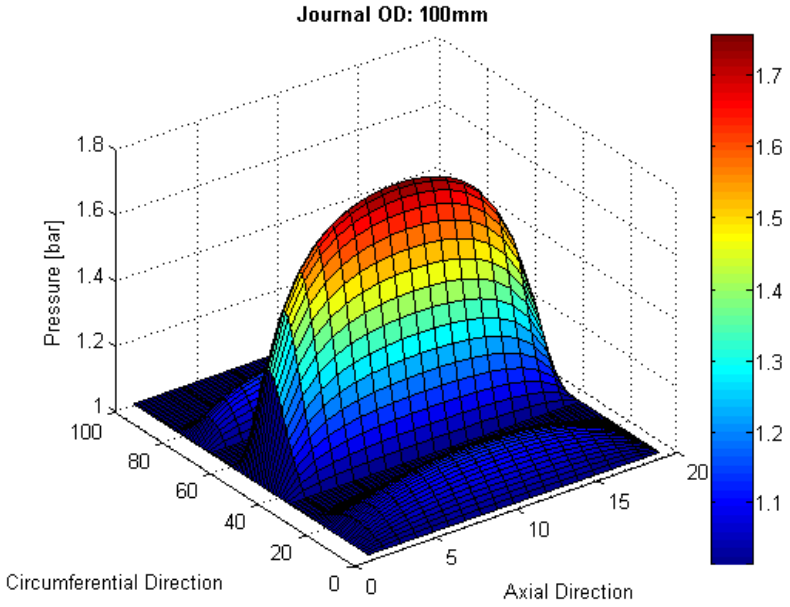

Figure 18 Pressure profile (Journal OD 100 mm and Speed 35 krpm)

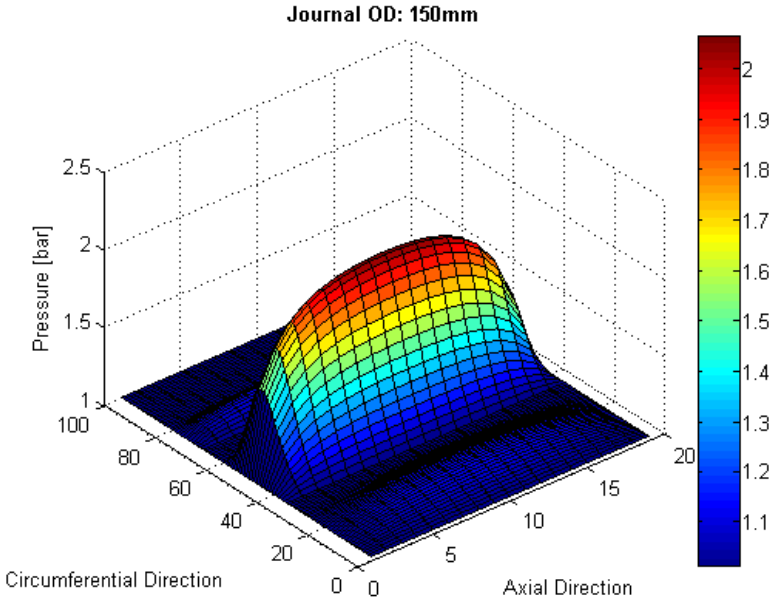

Figure 19 Pressure profile (Journal OD 150 mm and Speed 23.33 krpm)

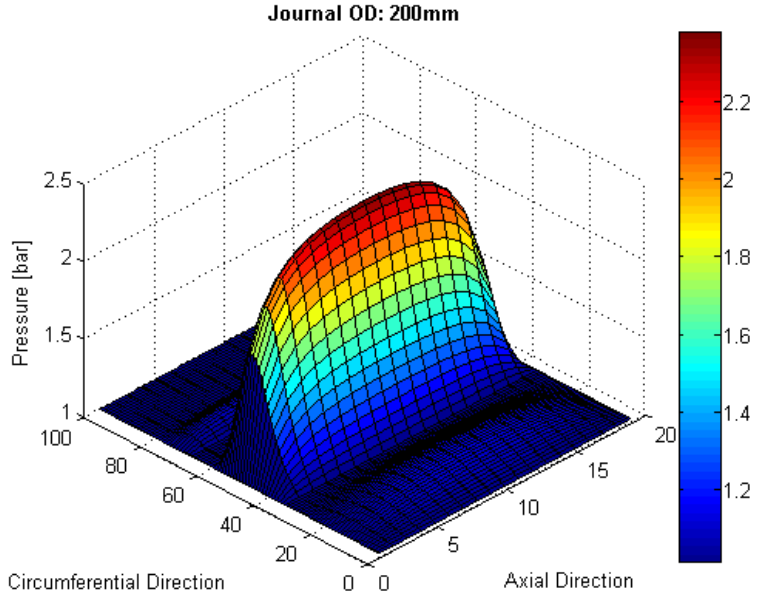

Figure 20 Pressure profile (Journal OD 200 and Speed 17.5 krpm)

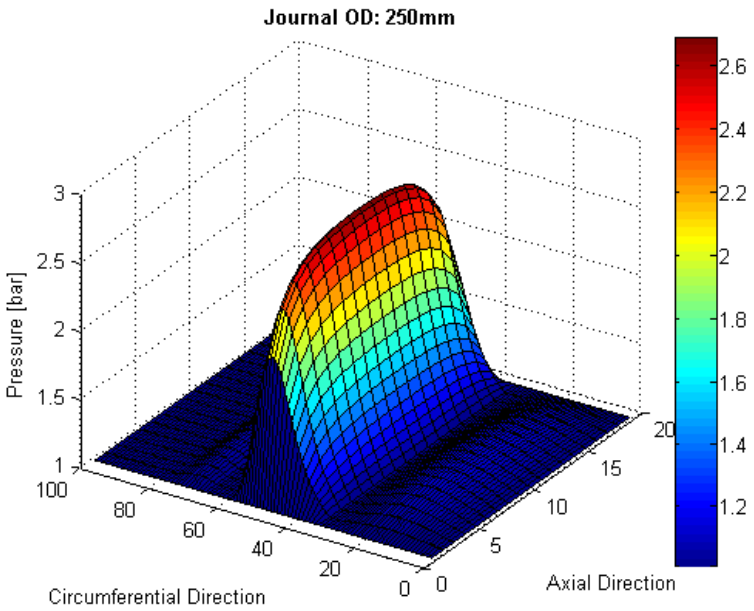

Figure 21 Pressure profile (Journal OD 250 mm and Speed 14 krpm)

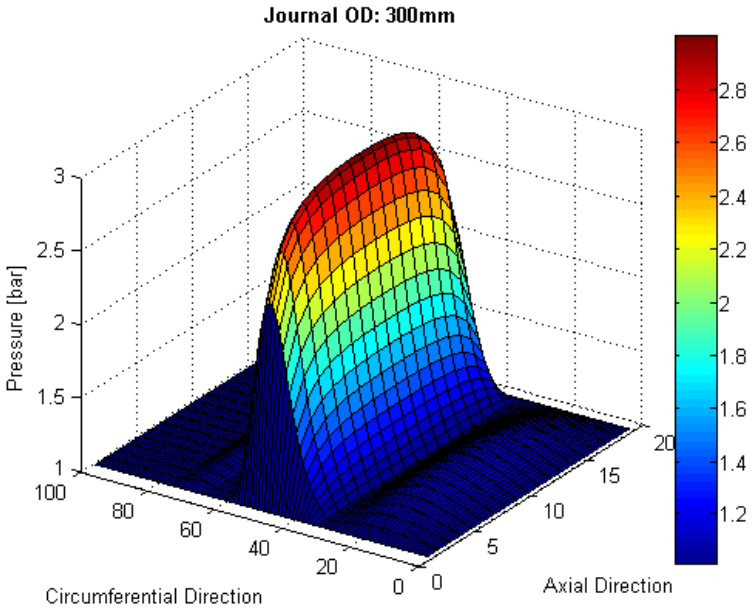

Figure 22 Pressure profile (Journal OD 300 mm and Speed 11.67 krpm)

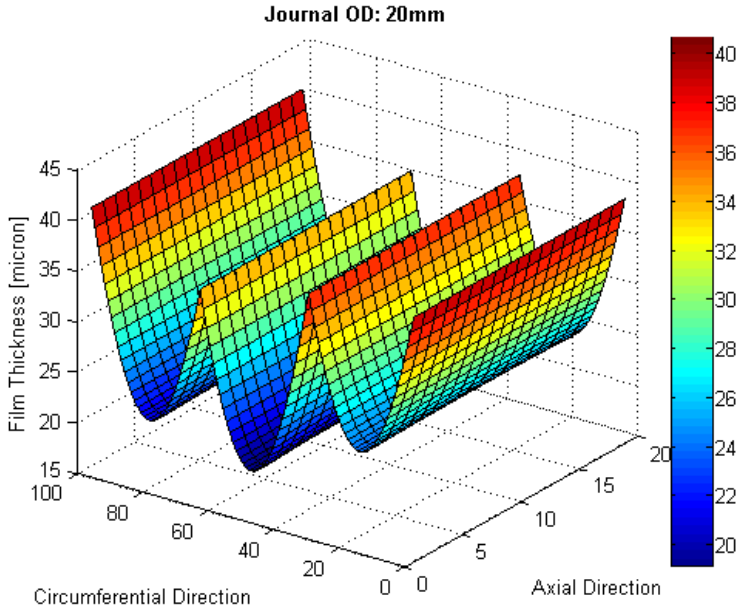

Figure 23 Film thickness (Journal OD 20 mm and Speed 175 krpm)

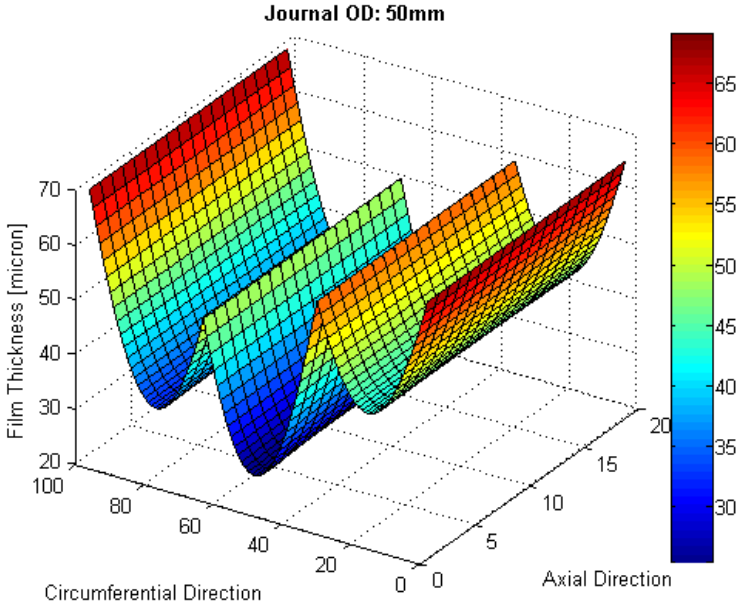

Figure 24 Film thickness (Journal OD 50 mm and Speed 70 krpm)

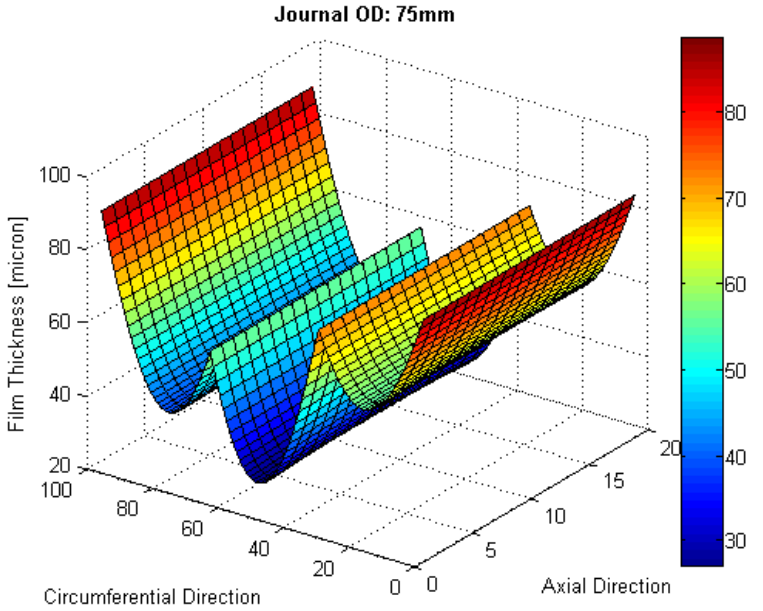

Figure 25 Film thickness (Journal OD 75 mm and Speed 46.67 krpm)

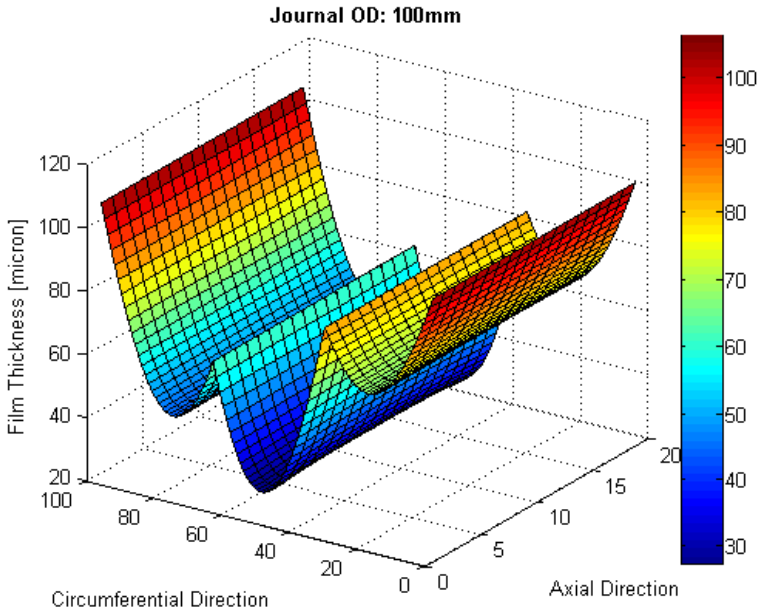

Figure 26 Film thickness (Journal OD 100 mm and Speed 35 krpm)

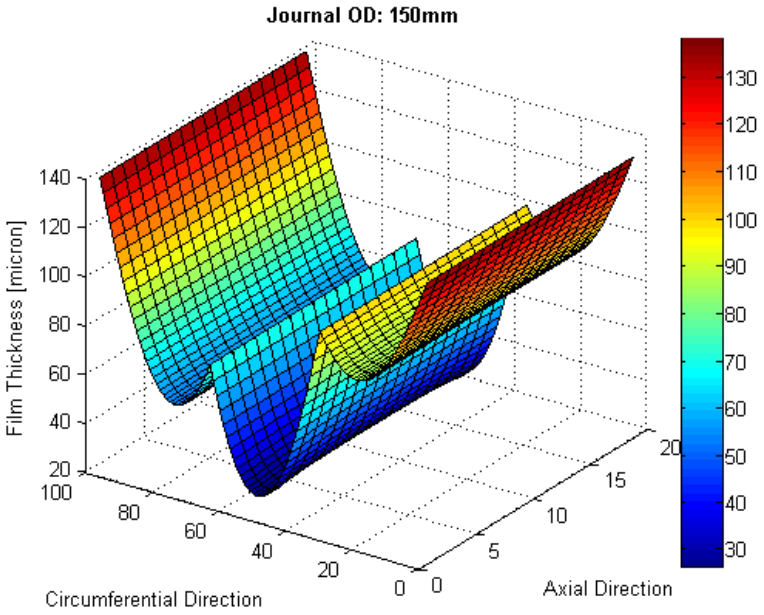

Figure 27 Film thickness (Journal OD 150 mm and Speed 23.33 krpm)

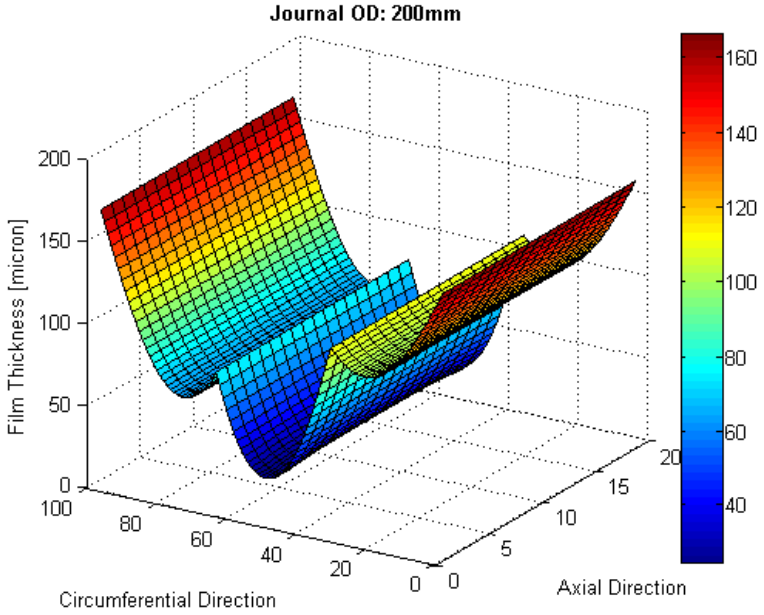

Figure 28 Film thickness (Journal OD 200 mm and Speed 17.5 krpm)

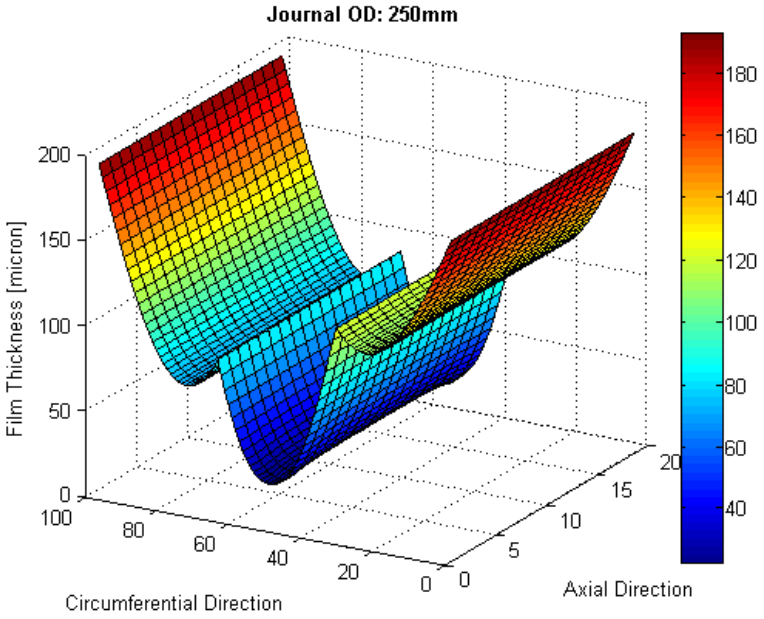

Figure 29 Film thickness (Journal OD 250 mm and Speed 14 krpm)

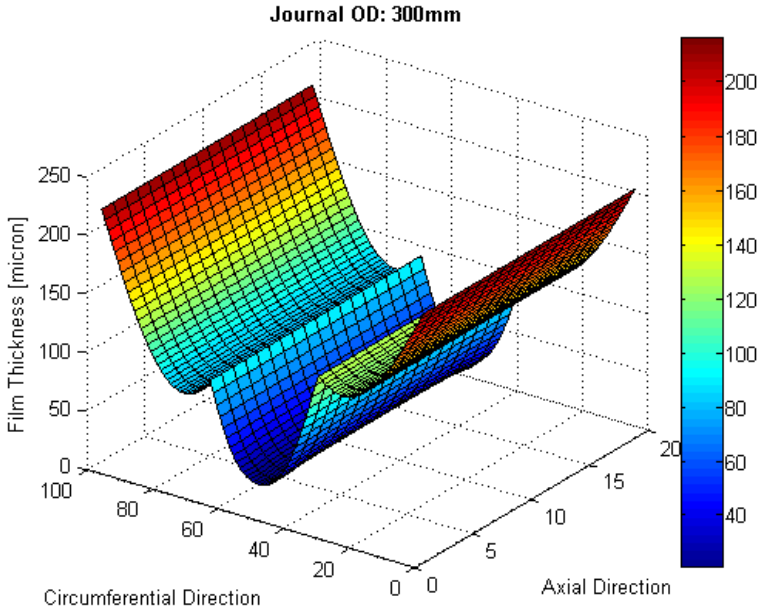

Figure 30 Film thickness (Journal OD 300 mm and Speed 11.67 krpm)

Table 6 Minimum film thickness and maximum pressure for all test cases

20 mm	H_min [μm]	P_max [bar]
35000	12.86	1.19
63000	15.88	1.21
91000	17.35	1.24
119000	18.21	1.27
147000	18.76	1.29
175000	19.12	1.32

50 mm	H_min [μm]	P_max [bar]
14000	12.69	1.43
25200	17.68	1.41
36400	20.80	1.42
47600	22.92	1.44
58800	24.36	1.45
70000	25.42	1.47

75 mm	H_min [μm]	P_max [bar]
9333	11.78	1.64
16800	17.18	1.60
24267	20.89	1.59
31733	23.57	1.59
39200	25.59	1.60
46667	27.12	1.61

100 mm	H_min [μm]	P_max [bar]
7000	10.86	1.84
12600	16.28	1.78
18200	20.25	1.76
23800	23.26	1.75
29400	25.59	1.75
35000	27.45	1.76

150 mm	H_min [μm]	P_max [bar]
4667	9.38	2.24
8400	14.39	2.15
12133	18.37	2.11
15867	21.58	2.08
19600	24.20	2.07
23333	26.36	2.06

200 mm	H_min [μm]	P_max [bar]
3500	8.23	2.62
6300	12.77	2.51
9100	16.53	2.46
11900	19.64	2.42
14700	22.27	2.39
17500	24.51	2.37

250 mm	H_min [μm]	P_max [bar]
2800	7.43	2.98
5040	11.43	2.86
7280	14.85	2.79
9520	17.81	2.75
11760	20.35	2.71
14000	22.56	2.69

300 mm	H_min [μm]	P_max [bar]
2333	6.81	3.34
4200	10.42	3.20
6067	13.49	3.13
7934	16.19	3.07
9800	18.56	3.03
11667	20.66	3.00

Chapter 6

CONCLUSIONS AND FUTURE WORK

A brief introduction to foil bearing technology was presented in Chapter 1. Review of pertinent literature was presented in Chapter 2 followed by the discussion on theoretical aspects of foil bearings in Chapter 3. The development of scaling laws and the methodology used for simulating the various test cases were presented in Chapter 4. Finally, the results of the simulations and the implications of scaling laws were presented in Chapter 5.

Scaling laws for radial foil bearings were developed using the scale invariant Reynolds equation and the NASA guideline for load capacity estimation [5]. From fundamental first principles, it was shown that the bearing radius is proportional to the square of the nominal clearance. Similarly, a power law relationship between the bearing radius and the bump stiffness was derived. It was found that bump stiffness is proportional to the bearing radius to the power of 1.5.

The implication of these scaling laws is that bump stiffness and nominal clearance for radial foil bearings can be estimated without resorting to detailed calculations. This thesis uses design guidelines from NASA [5] to establish functional relationship between bump stiffness and clearance with respect to the bearing radius. Similar concepts may be used in establishing bearing dynamic characteristics which would potentially accelerate the development of oil-free turbo-machinery systems.

This thesis was based on static analysis of foil bearings. Therefore, the results from this study serve as a guideline for bearing designers in making quick calculations of static parameters. In practical applications, the dynamic parameters including instability analysis play a vital role in the selection of bearings. Consequently, future work should be focused on development of scale laws related to dynamic parameters.

References

[1] Agrawal, G., L., 1997, "Foil Air/Gas Bearing Technology ~ An Overview," International Gas Turbine & Aero-engine Congress & Exhibition, Anonymous ASME, Orlando, Florida, **97-GT-347**.

[2] Piekos, E. S., February 2000, "Numerical Simulation of Gas-Lubricated Journal Bearings for Micro-fabricated Machines," Department of Aeronautics and Astronautics, MIT.

[3] Kim, D., Ki, J., Kim, Y., 2012, "Extended Three-Dimensional Thermo-Hydrodynamic Model of Radial Foil Bearing: Case Studies on Thermal Behaviors and Dynamic Characteristics in Gas Turbine Simulator," Journal of Engineering for Gas Turbines and Power, **134**(052501) pp. 1-13.

[4] Gross, W. A., July 1959, "A Gas Film Lubrication Study, Part 1, some Theoretical Analyses of Slider Bearings," IBM Journal, pp. 237-255.

[5] DellaCorte, C., and Valco, M., J., 2000, "Load Capacity Estimation of Foil Air Journal Bearings for Oil-Free Turbo-machinery Applications," NASA, NASA/TM-2000-209782, Ohio.

[6] Ausman, J. S., 1957, "Finite Gas Lubricated Journal Bearing," The Institute of Mechanical Engineers, Proceedings of the Conference on Lubrication and Wear, Anonymous pp. 39-45.

[7] Ausman, J. S., June 1961, "An Improved Analytical Solution for Self-Acting, Gas Lubricated Journal Bearings of Finite Length," Journal of Basic Engineering, **83(2)** (Trans of the ASME, Series D) pp. 188-194.

[8] Gross, W. A., and Zachmanoglou, E. C., June 1961, "Perturbation Solutions for Gas-Lubricated Films," Journal of Basic Engineering, **83(2)** (Trans. of the ASME, Series D) pp. 139-144.

[9] Gross, W. A., 1963, "Gas Bearings: A Survey," Wear, **6** pp. 423-443.

[10] Raimondi, A. A., 1961, "A Numerical Solution for the Gas-Lubricated Full Journal Bearing of Finite Length," ASLE Transactions, **4** pp. 131-155.

[11] Michael, W. A., July 1959, "A Gas Film Lubrication Study, Part 2, Numerical Solution of the Reynolds Equation for Finite Slider Bearings," IBM Journal, pp. 256-259.

[12] Carpino, M., and Talmage, G., 2003, "A Fully Coupled Finite Element Formulation for Elastically Supported Foil Journal Bearings," Tribology Transactions, **46**(4) pp. 560-565.

[13] Faria, M. T. C., and Andres, L., San, January 2000, "On the Numerical Modeling of High-Speed Hydrodynamic Gas Bearings," Journal of Tribology, **122** pp. 124-130.

[14] Cheng, H. S., and Pan, C. H. T., March 1965, "Stability Analysis of Gas Lubricated, Self-Acting, Plain, Cylindrical, Journal Bearings of Finite Length, using Galerkin's Method," Journal of Basic Engineering, **87(1)** (Trans of the ASME, Series D) pp. 185-192.

[15] Castelli, V., and Elrod, H. G., March 1965, "Solution of the Stability Problem for 360 Deg Self-Acting, Gas Lubricated Bearings," Journal of Basic Engineering, **87(1)** (Trans of the ASME, Series D) pp. 199-212.

[16] Elrod, H. G., and Burgdorfer, A., October 1959, "Refinements of the Theory of Infinitely-Long, Self-Acting, Gas-Lubricated Journal Bearing," First Intern. Symp. Gas-Lubricated Bearings, Anonymous Washington D. C., pp. 93-118.

[17] Stegen, vander, R. H. M., 1997, "Numerical Modelling of Self-Acting Gas Lubricated Bearings with Experimental Verification".

[18] Adams, G. G., July 1980, "Procedures for the Study of the Flexible-Disk to Head Interface," IBM Journal, **24**(4) pp. 512-517.

[19] Miller, B., and Green, I., January 1997, "On the Stability of Gas Lubricated Triboelements using the Step Jump Method," Journal of Tribology, **119** pp. 193-199.

[20] DellaCorte, C., Radil, K. C., Bruckner, R., Jack, 2008, "Design, Fabrication, and Performance of Open Source Generation 1 and 2 Compliant Hydrodynamic Gas Foil Bearings," Tribology Transactions, **51** pp. 254-264.

[21] Bruckner, R., Jack, August 2004, "Simulation and Modeling of the Hydrodynamic, Thermal and Structural Behavior of Foil Thrust Bearings".

[22] Heshmat, H., Walowit, J. A., and Pinkus, O., October 1983, "Analysis of Gas-Lubricated Foil Journal Bearings," Journal of Lubrication Technology, **105** pp. 647-655.

[23] Ku, R., C. P., and Heshmat, H., 1992, "Compliant Foil Bearing Structural Stiffness Analysis: Part 1 - Theoretical Model Including Strip and Variable Bump Foil Geometry," Journal of Tribology, **114(2)** pp. 394-400.

[24] Peng, J. P., and Carpino, M., January 1993, "Calculation of Stiffness and Damping Coefficients for Elastically Supported Gas Foil Bearings," Journal of Tribology, **115(1)** pp. 20-27.

[25] Carpino, M., January 1997, "Finite Element Approach to the Prediction of Foil Bearing Rotor Dynamic Coefficients," Journal of Tribology, **119** pp. 85-90.

[26] Salehi, M., Heshmat, H., and Walton, J., F., October 2003, "On the Frictional Damping Characterization of Compliant Bump Foils," Journal of Tribology, **125** pp. 804-813.

[27] Pan, C. H. T., and Kim, D., April 2007, "Stability Characteristics of a Rigid Rotor Supported by a Gas-Lubricated Spiral-Groove Conical Bearing," Journal of Tribology, **129** pp. 375-383.

[28] Song, J., and Kim, D., 2007, "Foil Bearing with Compression Springs: Analyses and Experiments," Journal of Tribology, **129(3)** pp. 628-639.

[29] Kim, D., 2007, "Parametric Studies on Static and Dynamic Performance of Air Foil Bearings with Different Top Foil Geometries and Bump Stiffness Distributions," Journal of Tribology, **129(2)** pp. 354-364.

[30] Kim, D., Creary, A., Chang, S. S., July 2009, "Meso-scale Foil Gas Bearings for Palm-Sized Turbo-machinery: Design, Manufacturing, and Modeling," Journal of Engineering for Gas Turbines and Power, **131**(042502) pp. 1-10.

[31] Kim, D., 2004, "Design and Fabrication of Sub-Millimeter Scale Gas Bearings with Tungsten-Containing Diamond Like Carbon Coatings".

[32] Moore, D. F., 1965, "A Review of Squeeze Films," Wear, **8**pp. 245-263.

[33] Powell, J. W., 1970, "A Review of Progress in Gas Lubrication," Review of Physics in Technology, **1**(2) pp. 96.

Biographical Information

Srikanth Honavara Prasad earned his Bachelor in Mechanical Engineering from the Visveswaraya Technological University, India, in 2008. He worked on computational modeling of hydrogen fuel cell systems and earned his Master of Science in Mechanical Engineering from the University of Texas at Arlington, USA, in 2010. Due to a broad interest in the field of transport phenomena in energy systems, he also pursued a Master of Science in Aerospace Engineering at the University of Texas at Arlington, USA. His interests include thermodynamics, heat transfer and computational fluid dynamics.